IEEE Access
Multidisciplinary ⋮ Rapid Review ⋮ Open Access Journal

Received 10 June 2024, accepted 8 August 2024, date of publication 19 August 2024, date of current version 29 August 2024.

Digital Object Identifier 10.1109/ACCESS.2024.3445913

RESEARCH ARTICLE

Estimation of Permittivity of Films Using the Free-Space Measurement Method at Ka-Band

DAEYEONG YOON[1], (Member, IEEE), JIHYUNG KIM[2], (Member, IEEE), DONG-YEOP NA[3], (Member, IEEE), AND YONG BAE PARK[1,4], (Senior Member, IEEE)

[1]Department of Electrical and Computer Engineering, Ajou University, Suwon-si, Gyeonggi-do 16499, South Korea
[2]Hanwha Systems, Yongin-si 17121, South Korea
[3]Department of Electrical Engineering, Pohang University of Science and Technology, Pohang-si 37673, South Korea
[4]Department of AI Convergence Network, Ajou University, Suwon-si, Gyeonggi-do 16499, South Korea

Corresponding author: Yong Bae Park (yong@ajou.ac.kr)

This work was supported in part by the Institute of Information and Communications Technology Planning and Evaluation (IITP) Grant funded by Korea Government (MSIT), Development of 3D-NET Core Technology for High-Mobility Vehicular Service, under Grant 2022-0-00704-001; and in part by the IITP Grant funded by Korea Government (MSIT) under Grant RS-2024-00396992.

ABSTRACT This work introduces a refined technique for the estimation of films permittivity within the Ka-band using free-space measurement method. Addressing the challenge of wrong solutions in permittivity estimation, our approach incorporates a frequency-dependent objective function, to find a unique estimation solution. We apply this technique to a variety of thin and flexible substrates, including cycloolefin polymer (COP), polyethylene terephthalate (PET), and polyimide (PI) films, and quantitatively analyze the uncertainty on the estimated permittivity and loss tangent. The proposed technique can offer a method for determining the permittivity of not only thin media but also flexible printed circuit boards used for circuits and antennas.

INDEX TERMS Free-space measurement, permittivity, thin layer, film, Ka-band.

I. INTRODUCTION

The increasing demand for mmWave technology, such as autonomous driving and 5G/6G networks, has led to a growing interest in the Ka-band frequency range [1], [2]. Consequently, accurate measurement of the permittivity of antenna materials used in this band has become crucial. Recent trends in antenna design have also shown an increased utilization of thin, transparent, and flexible films suitable for reconfigurable intelligent surfaces, optically transparent antennas, and origami antennas [3], [4], [5], [6]. Therefore, precise determination of the permittivity of these films within the Ka-band is essential for the design process.

Various studies have been conducted to estimate the permittivity of thin films. Resonance techniques are widely used to measure the permittivity of thin media and can accurately determine the permittivity and loss tangent. However, these methods provide results at a single frequency and require precise sample processing, which may not be suitable for non-specialized organizations [7], [8], [9]. To address these limitations, alternative methods can be employed. Waveguides can be used, but they may still require precise sample processing or additional structures such as electric band gap configurations [10]. Another approach is to use transmission lines [11] or coaxial lines [12] to estimate the sample's permittivity, which has the advantage of not requiring precise sample processing. However, these methods can be computationally intensive or yield inaccurate results due to the difficulty in numerical modeling when combined with full-wave techniques. Free-space measurement techniques may be the most suitable option for non-specialized organizations, as they offer versatility, eliminate the need for precise sample processing, and do not require extensive computational resources for permittivity estimation [13], [14], [15], [16], [17].

The free-space measurement technique involves measuring the reflection and transmission coefficients of a sample placed between two antennas connected to a VNA [18], [19], [20], [21]. This is a representative non-contact and non-destructive inspection method, which has the advantage of minimizing sample damage. By utilizing these characteristics, it is widely used for evaluating the reflection and

The associate editor coordinating the review of this manuscript and approving it for publication was Pavlos I. Lazaridis.

transmission performance of metasurfaces, frequency selective surfaces, radomes [22], [23]. It is also used to measure the permittivity of sheet materials, 3D printing materials, and films by accurately measuring the reflection and transmission coefficients. Furthermore, it can be used extensively in the fields of antennas and materials engineering because it can evaluate the performance of samples even in high-temperature environments [24]. To calibrate this system, the VNA's time gating is used, but it is provided as a paid option and may be difficult to use. However, the cost can be minimized by using the open source scikit-rf [25].

The Nicolson-Ross-Weir (NRW) method can be applied as a method of extracting the permittivity using free-space measurement technology. This method can estimate the permittivity using the S-parameter [26]. However, for media such as films, the reflection coefficient measurement may be inaccurate due to the ease of sagging [21]. This can lead to inaccurate permittivity estimation results. Therefore, accurate permittivity should be estimated using the transmission coefficient. To achieve this, an optimization method has been proposed that iteratively infers the permittivity to match the expected theoretical value with the measured observed value, resulting in a difference below a threshold value [17]. This method has the advantage of being very useful for estimating the permittivity of media. However, due to the periodicity of the exponential term of plane wave propagation at a single frequency, multiple solutions exist. If multiple solutions exist, the likelihood that the optimization algorithm will output an incorrect solution increases. Therefore, the objective function must be well defined to eliminate multiple solutions and output unique solutions.

In this paper, we provide a comprehensive overview of the hardware and software configurations used in free-space measurement techniques for measuring the permittivity of films in the Ka-band. Section II describes the hardware setup, the process of acquiring S-parameters, and the signal analysis of films. In Section III, we propose and explain an optimized objective function for determining the permittivity based on the film's signal analysis. We implement time gating using open-source software, implement the permittivity estimation algorithm using in-house code, and describe the process in detail. We then present the permittivity measurement results of various films, along with an analysis of measurement uncertainties, and discuss the findings. Throughout this paper, the time convention $e^{j\omega t}$ is consistently applied.

II. FREE-SPACE MEASUREMENT SETUP

A. HARDWARE CONFIGURATION

Measurements were conducted indoors at a temperature of 25.5°C and 42% humidity. The hardware setup for the free-space measurement is shown in Fig. 1. Two focusing lens horn antennas (Anteral's FLHA-28) are mounted on a rail and stage, allowing for movement along the rail axis. The antennas are connected to a vector network analyzer (VNA, Rohde & Schwarz ZVA67) through phase stable cables (Withwave WT100) and WR28 to coaxial adaptors

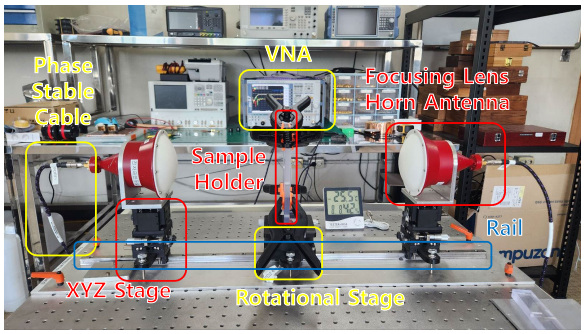

FIGURE 1. Hardware configuration of free-space measurement method.

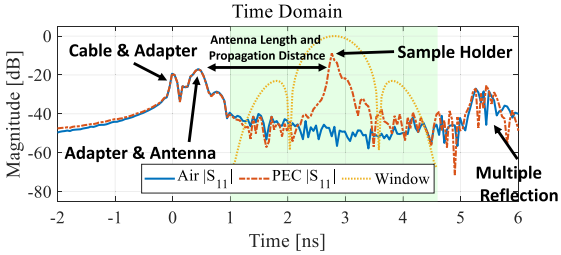

FIGURE 2. Signal separation from material holder using time gating.

(Eravant SWC-28KF-E1-T). These antennas generate a Gaussian beam, which propagates in a quasi-plane wave [16], [17]. The sample holder is positioned on a rotational stage above the rail, enabling rotation along the rail axis and angle adjustment using the rotational stage. The VNA is connected to a personal computer (PC) via a local area network (LAN) and is configured for remote scattering coefficient acquisition through Python's pyVISA.

The material holder is made of acrylic and has a square hole of 100 × 100 mm^2 inside. This is significantly larger than the 3 dB beam waist of 13.1mm (at E-plane) and 16.9mm (at H-plane) of the antenna we used. It is established that when the material's size is approximately 3 to 5 times the diameter of the antenna's beam waist, diffraction effects occurring at the holder's corners can be disregarded [17]. In the above configuration, measurements of horizontal and vertical polarization can also be performed by changing the orientation of the antenna. In this paper, measurements are performed for vertical polarization.

B. TIME-GATING PROCESS

Due to the influence of the cables and adapters connecting the antenna and the VNA, the acquired scattering coefficients include undesired multiple reflection signals. To obtain the inherent scattering coefficients of the sample, the time-gating technique is employed. This technique involves transforming the frequency-domain signal into the time domain via inverse fast Fourier transform (IFFT) for analysis, and then multiplying by a window function in the time domain to eliminate all unwanted reflection signals [13], [15].

To perform time-gating, calibration with the cables connected to the VNA was initially carried out. Subsequently,

scattering coefficients were acquired with no material in the holder (AIR) and with a metal reflector present (PEC, like a perfect electric conductor). The time-domain transformation results are as shown in Fig. 2. At 0 ns and approximately 0.5 ns in Fig. 2, peaks are observed for both AIR and PEC, which can be attributed to transitions between the cable and adapter, and the adapter and antenna, respectively. Additionally, a smaller peak around 5.2 ns is identified, likely due to multiple reflections. Conversely, a pronounced peak for PEC is noticeable at about 2.7 ns, which can be distinguished as the sample region. The distance from the transition between the adapter and antenna to the sample holder can be identified by the antenna length and the propagation distance. Therefore, a window function was defined to preserve the signal in this region and remove all other signals. A flattop window function, which minimizes variation ripple, was utilized. The open source scikit-rf [25] was used for time gating.

Applying the window function in the time domain through multiplication is equivalent to convolution operation in the frequency domain. The convolution operation in the frequency domain leads to signal distortion at the start and end points of the frequency band, known as the edge effect [27]. To mitigate this, measurements were conducted over a slightly broader range (22 - 44 GHz) than the area of interest (26 - 40GHz), and frequencies outside the interested band were trimmed. Here, 22 GHz represents the cut-off frequency of WR28, and 44 GHz is the limit frequency of the 2.92mm calibration kit (Rohde & Schwarz ZV-Z129E).

C. CALIBRATION OF THE SCATTERING COEFFICIENTS

To calibrate the scattering coefficients of the sample, three signal acquisitions are necessary: with nothing installed on the sample (AIR), with a metal reflector installed (PEC), and with the sample installed (MUT, material under test). After eliminating unwanted reflection coefficients using the time-gating technique for these three signals, the scattering coefficients are calculated using the following equations by [15], [28],

$$S_{11}^{MEA} = \frac{S_{11}^{MUT} - S_{11}^{AIR}}{S_{11}^{AIR} - S_{11}^{PEC}} \tag{1a}$$

$$S_{21}^{MEA} = \frac{S_{21}^{DUT} - S_{21}^{PEC}}{S_{21}^{AIR} - S_{21}^{PEC}} e^{-j\beta_0 t_{MUT}} \tag{1b}$$

where t_{MUT} is the thickness of the MUT, β_0 is the wave number in free-space. In Eq. (1b), involves phase correction for the thickness of the sample. This correction allows for the elimination of the need to physically move the antenna by the thickness of the sample.

The subsequent measurement process was conducted as follows: The VNA was connected to the antenna via cables, and calibration was performed between the VNA and the cables before measurements. After connecting the cables to the antenna, the scattering coefficients for AIR, PEC, and MUT were acquired. Following this, reflection and transmission coefficients were calculated using Eq. (1).

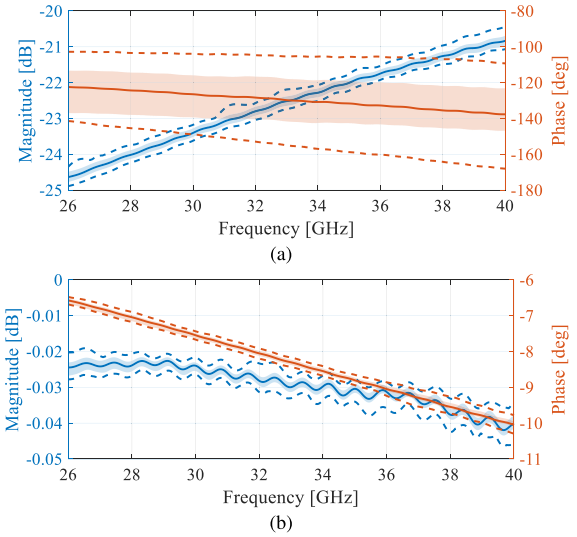

FIGURE 3. The uncertainty in PI100 coefficients. The shaded area represents the standard deviation, and the dotted lines represent the maximum and minimum values. (a) Reflection coefficient (b) Transmission coefficient.

TABLE 1. Standard deviation of reflection and transmission coefficients for each sample.

Material	$\lvert S_{11}\rvert$ [dB]	$\angle S_{11}$ [deg]	$\lvert S_{21}\rvert$ [dB]	$\angle S_{21}$ [deg]
COP	0.0978	17.5	0.0013	0.0912
PET	0.0497	37.7	0.0017	0.0891
PI100	0.391	3.02	0.0012	0.0856
PI50	0.086	3.60	0.0014	0.0747
PI25	0.133	11.9	0.0013	0.0735

D. ANALYSIS OF UNCERTAINTY IN SCATTERING COEFFICIENTS

There are uncertainties associated with the VNA and specimen during the S-parameter measurement process. The S-parameter measurement uncertainty of the VNA can be determined by referring to the datasheet. When the S_{11} signal is between -25 and -35 dB, the measurement uncertainty is less than 3 dB for magnitude and 20 degrees for phase. When the S_{21} signal is between $+5$ and -45 dB, the measurement uncertainty is less than 0.2 dB for magnitude and 2 degrees for phase. In addition to the VNA's uncertainty, there may be uncertainty due to the sagging of the film specimen. To analyze the combined effect of these uncertainties, the measurement uncertainty for reflection and transmission coefficients was evaluated. The experimental standard deviation of the reflection and transmission coefficients, denoted as $s(S_{ij}^k)$, indicates the level of uncertainty in the observed values and is defined by [29]

$$s(S_{ij}^k) = \sqrt{\frac{1}{n-1}\sum_{k=1}^{n}(S_{ij}^k - \bar{S}_{ij})^2} \tag{2}$$

where $\bar{S}_{ij}$ represents the arithmetic mean of the n times acquired scattering coefficients, calculated as the average of the measurements S_{ij}^k:

$$\bar{S}_{ij} = \frac{1}{n}\sum_{k=1}^{n} S_{ij}^k \tag{3}$$

The analysis focused on both the amplitude and phase of the reflection and transmission coefficients for the MUTs. The experiment was repeated $n = 100$ times, with 5 cycles of installing and removing the specimen and obtaining 5 signals from the VNA in each cycle. Measurements were conducted on 4 samples of the same type. For instance, the standard uncertainty results for a polyimide film with a thickness of 100μm (PI100) are depicted in Fig. 3. The shaded area in Fig. 3 indicates the standard deviation, the dotted lines show the maximum and minimum measurement values, and the solid line represents the mean value, where blue denotes magnitude and red denotes phase. Additionally, the standard deviation of the uncertainty is as shown in Table 1. Here, the standard deviation is indicated as the mean value across frequencies. Information about the measured samples is specifically described in section IV-A.

Comparing the data in Fig. 3 or Table 1, it is evident that the uncertainty in the phase of the reflection coefficients is substantially larger than that in the transmission coefficients. In some specimens, the phase uncertainty of S_{11} is observed to be much larger than the uncertainty presented in the VNA datasheet. This shows that accurate estimation of the reflection coefficient is difficult due to specimen deflection as well as the uncertainty of the VNA. Conversely, the uncertainties in the transmission coefficients are not as significant and show consistency across different samples. Thus, when estimating the permittivity, it is advisable to rely on the average of the transmission coefficients (S_{21}), which exhibit relatively lower uncertainty.

III. PERMITTIVITY ESTIMATION METHOD

The principle of the permittivity estimation technique used in this study involves expressing the expected theoretical values as a function of the permittivity and finding the permittivity that minimizes the difference between these theoretical values and the actual measurements. An optimization technique is utilized to quickly identify the point of minimum difference.

A. THEORETICAL VALUE CALCULATION

To use the optimization technique, the expected theoretical values must first be expressed as a function of the complex relative permittivity (ε_r). Theoretically, as shown in Fig. 4, the estimated theoretical value S_{21}^{est} when a plane wave is incident at a specific angle to the homogeneous film is given by Eq. (4) [30]. This is expressed as a geometric series sum of the transmission coefficients in region 2, the transmission area.

$$S_{21}^{est}(f, \varepsilon_r) = T = \frac{t_{01}t_{12}e^{-j\beta_1 \cos\theta_1 d_1}}{1 - r_{10}r_{12}e^{-j2\beta_1 \cos\theta_1 d_1}} \tag{4}$$

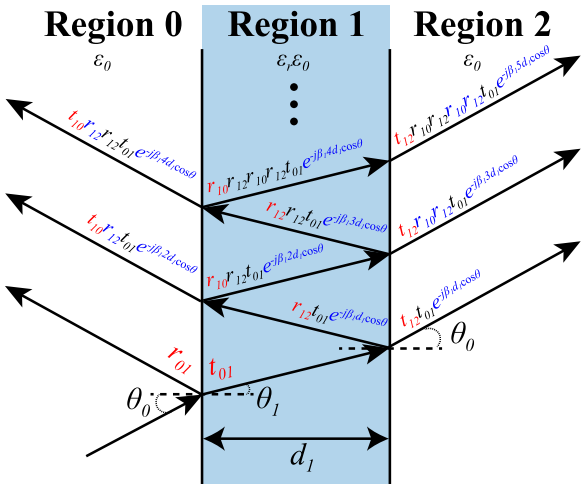

FIGURE 4. Plane wave propagation through a homogeneous film. The red text represents terms newly defined due to reflection and transmission, while the blue text signifies geometric progression. Additionally, the described equations represent the coefficients at the starting point of the arrows.

where $\beta_1 = 2\pi f\sqrt{\varepsilon_r}/c$ (where f is frequency and c is the speed of light), d_1 represents the thickness of the sample, and θ_1 denotes the angle of transmission. Additionally, $r_{ab}$and t_{ab} represent the reflection and transmission waves at the boundary between media a and b, and are summarized as

$$r_{01} = r_{21} = -r_{10} = -r_{12} = \frac{\cos\theta_0 - \sqrt{\varepsilon_r}\cos\theta_1}{\cos\theta_0 + \sqrt{\varepsilon_r}\cos\theta_1} \tag{5}$$

$$t_{01} = t_{21} = \frac{2\cos\theta_0}{\cos\theta_0 + \sqrt{\varepsilon_r}\cos\theta_1} \tag{6}$$

$$t_{10} = t_{12} = \frac{2\cos\theta_1}{\cos\theta_0 + \sqrt{\varepsilon_r}\cos\theta_1} \tag{7}$$

where θ_0 is the angle of incidence at region 0. The angle of transmission θ_1 in region 1 is calculated from Snell's law by

$$\theta_1 = \sin^{-1}\left(\frac{1}{\sqrt{\varepsilon_r}}\sin\theta_0\right) \tag{8}$$

The angle of incidence and the thickness of the sample indicated in Eq. (4) are determined before measurement. Therefore, Eq. (4) is a function of frequency and the permittivity, with other variables being constants.

B. OBJECTIVE FUNCTION DEFINITION

As discussed in the previous section, significant uncertainty in reflection was observed. Therefore, the objective function needed for the optimization operation utilizes the transmission coefficients. The designed objective function $g(\varepsilon_r)$ is as follows:

$$g(\varepsilon_r) = g(\varepsilon_r', \varepsilon_r'') = |S_{21}^{est}(\varepsilon_r', \varepsilon_r'') - S_{21}^{mea}| \tag{9}$$

Based on this designed objective function, the point where the objective function is minimized at each frequency is searched. The designed objective function performs the optimization operation as a function of two variables, the real part (ε_r') and the imaginary part (ε_r'') of the complex permittivity. The real

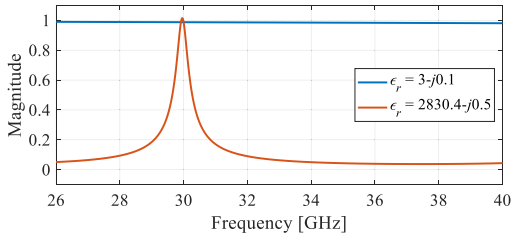

FIGURE 5. This show that there can be more than two permittivity with similar transmission coefficients at a single frequency (30 GHz).

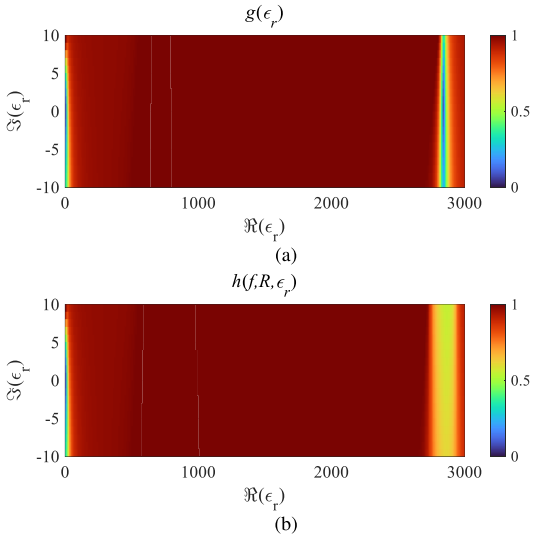

FIGURE 6. Comparison of objective function performance demonstrates that by adding a comparison over a frequency range R, it is possible to reduce the number of local minima to one.

and imaginary parts of the complex permittivity are defined as follows, and the loss tangent is denoted as the ratio of the imaginary part to the real part.

$$\varepsilon_r = \varepsilon_r' - j\varepsilon_r'', \quad \tan\delta = \frac{\varepsilon_r'}{\varepsilon_r''}$$

However, due to the periodicity of the exponential term in Eq. (4) ($e^{j\phi} = e^{j(\phi\pm 2\pi)} = e^{j(\phi\pm 4\pi)} = \cdots$), the objective function in Eq. (9) may show redundant results for the estimated permittivity. This is illustrated in Fig. 5, where the actual permittivity is assumed to be $3 - j0.1$, and the redundant permittivity value $(2830.4 + j0.5)$ at 30 GHz matches only within a very narrow range. Based on this observation, an objective function $h(f, R, \varepsilon_r)$ was formulated by adding frequency (f) for comparison of measurement results over a frequency range (R) as follows. It sums up the differences between measured and predicted values within the range from $f - R/2$ to $f + R/2$:

$$h(f, R, \varepsilon_r) = \sum_{f_i=f-R/2}^{f+R/2} |S_{21}^{est}(f_i, \varepsilon_r', \varepsilon_r'') - S_{21}^{mea}(f_i)| \qquad (10)$$

Fig. 6a shows the results when the objective function is adopted as Eq. (9) at 30 GHz. When adopting the objective function as Eq. (9), it can be observed that the permittivity has

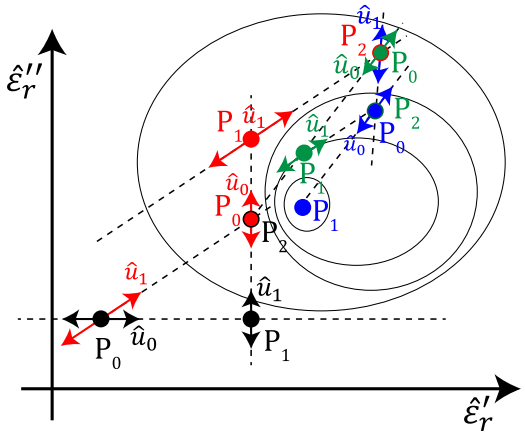

FIGURE 7. Powell's method in two-dimensional plane.

local minima at about 3 and 2830. These numerical defects cause instability not only in thin samples but also in thick samples, and can lead to unstable results when applying the optimization function. In contrast, Fig. 6b shows the results when adopting the objective function as Eq. (10). Here, the value of R was set to 1 GHz, specifically comparing the range of 29.5 to 30.5 GHz. It can be observed that, unlike Fig. 6a, the local minimum exists only near 3. Thus, by comparing the results at a specific frequency, the stability of permittivity estimation during the optimization process can be ensured.

C. OPTIMIZATION METHOD

To solve the optimization problem, the value of the objective function must be minimized. Powell's conjugate method [31], [32] was used to find the real and imaginary parts of the permittivity at which the objective function is minimized. This method is known to be able to stably find the optimal value even when the function is of a complex form, as it does not use the derivative of the function to find the minimum. The principle of this technique in two dimensions is as follows [32] and depicted in Fig. 7.

- Save your starting position as P_0.
- Move P_0 to the minimum point along direction $\hat{u}_0$ and call this point P_1. Here, P_1 is the minimum value in the direction of $\hat{u}_0$.
- Move P_1 to the minimum point along direction $\hat{u}_1$ and call this point P_2. Here, P_2 is the minimum value in the direction of $\hat{u}_1$.
- Set u_0 to u_1
- Set u_1 to $P_2 - P_0$
- MoveP_2 to the minimum along direction $\hat{u}_1$ and call this point P_0.

This process is repeated until the difference between P_0 and P_2 converges to a preset minimum threshold. In Fig. 7, the first step is indicated in black, the second step in red, the third step in green, and finally, the fourth step in blue, illustrating the aforementioned method. The optimization process involves finding a minimum in one direction. When using the objective function in Eq. (9), the

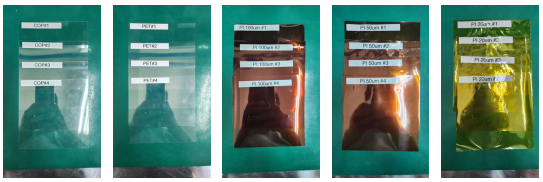

FIGURE 8. Photos of the measured samples (a) COP, (b) PET, (c) PI100, (d) PI50, (e) PI25. Although labeled as PI 20μm in the figure, the actual measured thickness is 25μm.

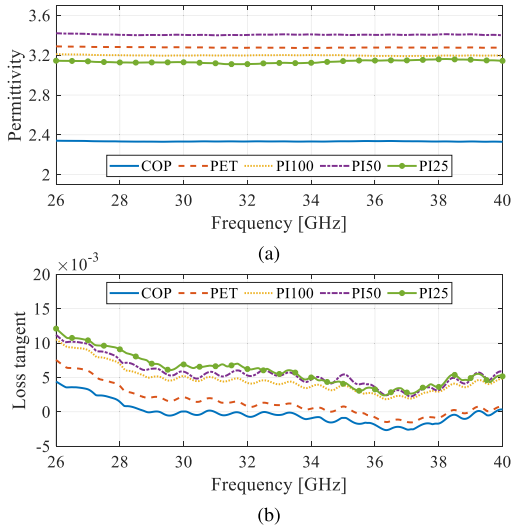

FIGURE 9. Complex permittivity estimation results (a) Permittivity (b) Loss tangent.

desired output may not be achieved. Therefore, by adding a term that compares different frequencies as in Eq. (10), it was possible to partially overcome the divergence of the optimization algorithm. We implemented the optimization technique using the optimize library in Python's SciPy [33], with the minimum for convergence set to 1×10^{-6}.

IV. PERMITTIVITY ESTIMATION RESULTS

A. PERMITTIVITY ESTIMATION SAMPLES

The permittivity of the samples, as shown in Fig. 8, was estimated using the proposed method. These samples include COP(Zeon ZF14), PET(SKC V7610), and PI(SKC IN70) films. The thickness of the COP and PET films is 188μm, while the PI films have thicknesses of 100μm, 50μm, and 25μm. Although labeled as PI 20μm in the Fig. 8, the actual thickness was 25μm. To easily distinguish these samples, they were named PI100, PI50, and PI25, respectively. The thickness of the samples was measured using a Mitutoyo thickness gauge (293-230-30), with a measurement error of 1μm.

B. PERMITTIVITY ESTIMATION RESULTS

As shown in Fig. 3b, the permittivity was estimated based on the average of several transmission measurements and the proposed method. The results are presented in Fig. 9. In Fig. 9, the average permittivity and loss tangent for COP are (2.33, -2.16$\times10^{-4}$), for PET (3.28, 1.36$\times10^{-3}$), and for PI100, PI50, and PI25, they are (3.20, 4.65$\times10^{-3}$), (3.41, 5.54$\times10^{-3}$), and (3.14, 6.00$\times10^{-3}$), respectively. The representative values are expressed as the average across frequencies. COP and PET are shown to have negative values in some sections. This can be attributed to uncertainty due to measurement, which will be addressed in the following section.

To verify the accuracy of the estimated permittivity values, theoretical values were reconstructed based on the estimated permittivity. For instance, the results for the samples are shown in Fig. 10. When comparing the restored transmission coefficients with the measurements, it is evident that the fluctuations due to time-gating are somewhat mitigated due to the objective function's R (1GHz), reflecting the trend in transmission rates. The reflection coefficients show a discrepancy of about 0.2 dB for all samples. Despite estimating the permittivity using transmission rates due to the inaccuracies in measuring reflection coefficients, there is no significant difference. This trend is consistent across all samples, thereby validating the effectiveness of the proposed technique.

C. UNCERTAINTY OF PERMITTIVITY ESTIMATION

It has been identified that a total of four factors influence our permittivity estimation system. These are the angle of incidence of the sample, uncertainty in the magnitude and phase of the VNA transmission coefficients, and thickness estimation uncertainty. Among these factors, the magnitude and phase of the VNA transmission coefficients were set to values with a 95% confidence level, specifically twice the values listed in Table 1. The error in the angle of incidence and thickness estimation was set based on the stage's angular error (0.5 degrees) and the thickness gauge's measurement error (1μm), respectively. The permittivity estimation uncertainty was analyzed using the root mean square tolerance analysis [34] as

$$\Delta X = \sqrt{\Delta X_\theta^2 + \Delta X_{|S_{21}|}^2 + \Delta X_{\psi_{21}}^2 + \Delta X_t^2} \tag{11}$$

here, ΔX_y is a partial differential with respect to y and is calculated as

$$\Delta X_y = \frac{\partial X}{\partial y} \Delta y$$

where X represents ε_r' and $\tan\delta$, θ is the angle of incidence of the sample, $|S_{21}|$ is the magnitude of the transmission coefficient, ψ_{21} is the phase of the transmission coefficient, and t is the thickness of the sample. Each elements and its sums are shown in Fig. 11.

Fig. 11a shows the permittivity estimation uncertainty for COP. The uncertainty of COP loss tangent is larger than the measured loss tangent in some frequency ranges. This indicates that it can have negative value. All samples exhibit a tendency for uncertainty to decrease as the frequency increases. To clearly analyze the impact based on the type of sample, the average uncertainty across the frequency band is represented in bar graph form as shown in Fig. 11b and 11c.

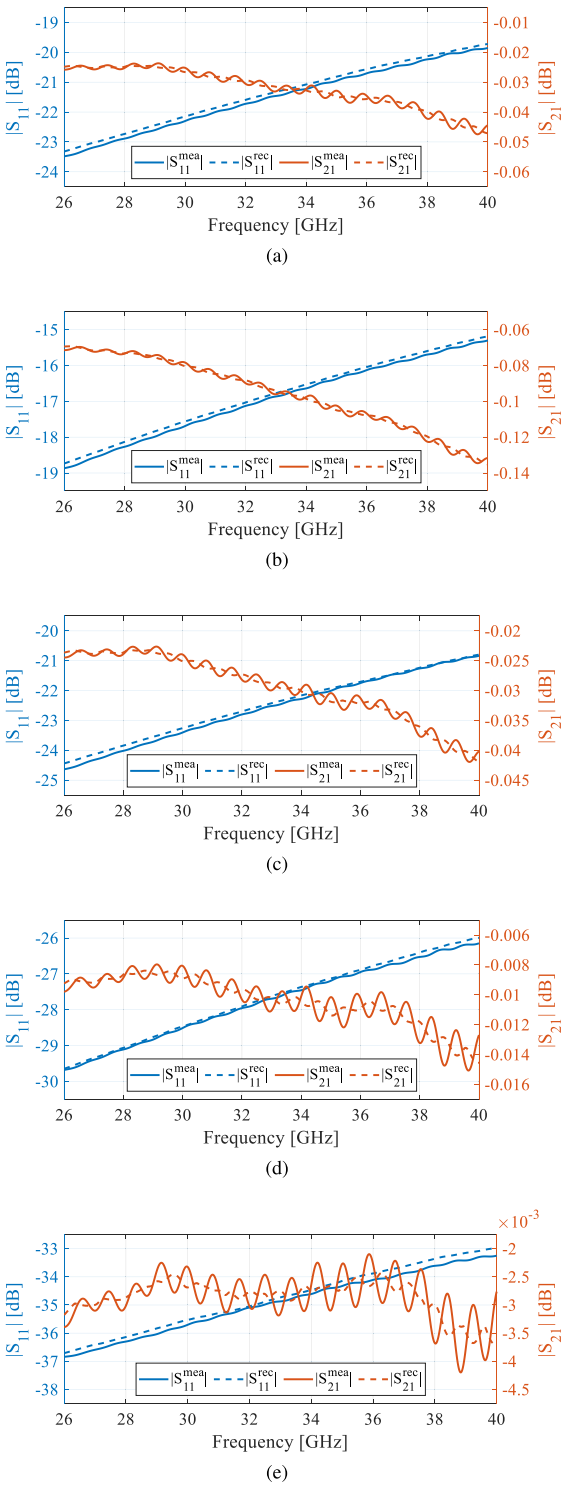

FIGURE 10. Reconstruction of S-parameters from the estimated permittivity (a) COP (b) PET (c) PI100 (d) PI50 (e) PI25.

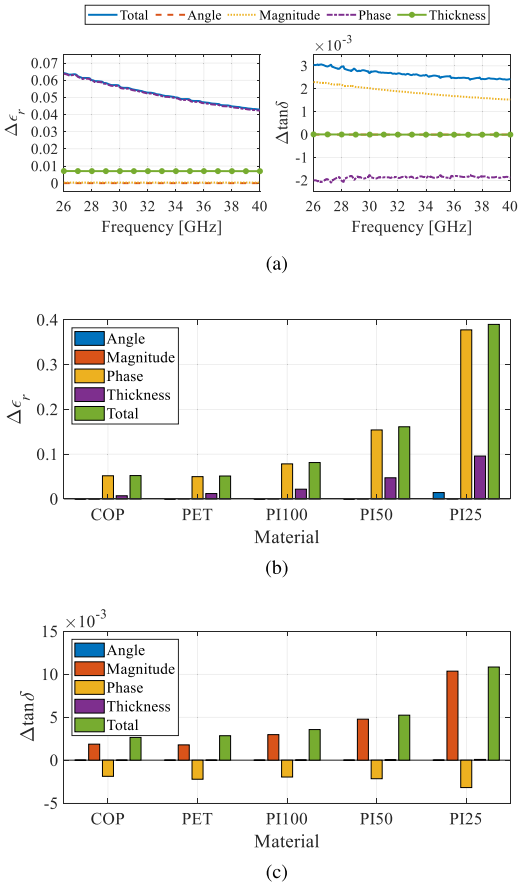

FIGURE 11. Permittivity estimation uncertainty for films (a) Uncertainty of COP film at Ka-band, (b) Average relative permittivity uncertainty, (c) Average loss tangent estimation uncertainty.

In Fig. 11b, the largest uncertainty factor in permittivity estimation is the phase of the transmission coefficient. In Fig. 11c, the magnitude of the transmission coefficient is the most significant factor affecting the uncertainty of the loss tangent estimation. Additionally, the uncertainty tends to increase for thinner films. This is because the magnitude of the transmission coefficient decreases for thinner films, while the uncertainty of the transmission coefficient, as shown in Table 1, remains constant regardless of the sample. These results highlight the importance of measurement procedure that can minimize the uncertainty of the transmission coefficient.

D. DISCUSSION

We compared our measurement results with those of other studies, as shown in Table 2. In the study using a balanced circular-disk resonator for broadband complex permittivity measurements of COP (thickness is 200μm) [9], the permittivity and loss tangent were (2.325, 6.3×10^{-4}), with an uncertainty of (5.1e-3, 9.7×10^{-5}). This study measured the permittivity using the characteristic that the TM_{0m0} mode is selectively excited in a circular resonator, requiring a circularly processed film. As the results show, it provides very precise outcomes for measuring low-loss materials in film type. However, this technique requires the sample to be processed into various sizes of circular shapes and necessitates circular-shaped conductor films. This could lead to measurement errors if the machining is not precise. Although measurements can be made across a wide frequency range, there is a limitation on the number of measurable

TABLE 2. Comparison of measurement results with other studies.

Reference	Contribution	Material	Permittivity (Uncertainty*1)
[9]*1	The complex permittivity measurement and uncertainty evaluation of low-loss COP films using a broadened frequency measurement range balanced-type circular disk resonator technique.	COP (200um)	ϵ_r=2.325 (5.1×10^{-3}) tan δ=6.3×10^{-4} (9.7×10^{-5})
[35]*2	Measurement of the permittivity of films at ultra-wideband and various temperatures using the free-space measurement method.	PET (107um)	ϵ_r=3.45 tan δ=1.74×10^{-2}
		PI (50um)	ϵ_r=3.60 tan δ=5.0×10^{-2}
Our Works*1,3	Measurement and uncertainty evaluation of the complex permittivity of various films using the free-space measurement method. Overcame potential instabilities in optimization techniques.	COP (188 um)	ϵ_r=2.33 (5.2×10^{-2}) tan δ=-2.16×10^{-4} (2.6×10^{-3})
		PET (188 um)	ϵ_r=3.28 (5.1×10^{-2}) tan δ=1.36×10^{-3} (2.8×10^{-3})
		PI (100 um)	ϵ_r=3.20 (5.1×10^{-2}) tan δ=4.64×10^{-3} (3.6×10^{-3})
		PI (50 um)	ϵ_r=3.40 (1.6×10^{-1}) tan δ=5.54×10^{-3} (5.2×10^{-3})
		PI (25 um)	ϵ_r=3.13 (3.9×10^{-1}) tan δ=6.00×10^{-3} (1.1×10^{-2})

*1 Based on a 95% confidence level.
*2 Permittivity and loss tangent values at room temperature and at 33 GHz.
*3 Values are presented as averages within the Ka-band range.

frequency points. If measurements at specific frequencies are needed, techniques such as interpolation would have to be employed.

On the other hand, the study from [35] measured the permittivity of PET (thickness is 107μm) and PI (thickness is 50μm) films using the free-space measurement method. This study presented results analyzing the change in permittivity of films with temperature. However, it lacks analysis on precision and uncertainty, which is a limitation.

Our proposed method measured the permittivity using the free-space measurement method and conducted measurements with a procedure capable of high precision. Additionally, the proposed configuration can be implemented cost-effectively using scikit-rf [25], an open source library. The proposed technique can also be applied to measure the permittivity of materials with some thickness (such as wood, plastic, concrete, etc.), not just films [36]. Furthermore, precisely machined samples are not required in the measurement process. Therefore, the impact on the uncertainty of measurements is minimized. To do this, one can try a method that does not apply time gating [17] or apply VNA error terms calibration method such as Thru-Reflect-Line [18] and Gated-Reflect-Line [13], [20]. Moreover, measurements are conducted at finely spaced intervals of 10 MHz within the Ka-band, which effectively eliminates the need for interpolation methods and facilitates more accurate estimations of permittivity. However, there are some limitations in evaluating low-loss materials due to the uncertainty of the transmission coefficient. Therefore, measurement methods that can developed the impact of the uncertainty of the transmission coefficient should be proposed. Moreover, since films have different permittivity at various temperatures [35], studies on the material properties of media under conditions of temperature change should also be conducted.

V. CONCLUSION

Throughout this study, the process of estimating the permittivity of films in the Ka band using free-space measurement was investigated, and the measurement uncertainty was examined. Implementation costs were reduced by utilizing open-source software for system calibration. The accuracy and reliability of the optimization algorithm were improved by deriving a unique solution using a frequency-dependent objective function. The permittivity and loss tangent of thin and flexible substrates such as COP, PET, and PI films were estimated, and the influence of factors affecting the results was analyzed through measurement uncertainty analysis. Additionally, the study results were verified by reconstructing the measurements and comparing them with other studies. The proposed technique could provide a method for determining the permittivity of not only thin media but also flexible printed circuit boards used in circuits and antennas.

REFERENCES

[1] S. F. Jilani, Q. H. Abbasi, and A. Alomainy, "Inkjet-printed millimetre-wave PET-based flexible antenna for 5G wireless applications," in *IEEE MTT-S Int. Microw. Symp. Dig.*, Aug. 2018, pp. 1–3.

[2] R. Liu, J. Dou, P. Li, J. Wu, and Y. Cui, "Simulation and field trial results of reconfigurable intelligent surfaces in 5G networks," *IEEE Access*, vol. 10, pp. 122786–122795, 2022.

[3] J.-Y. Lee, S. Jung, Y. Youn, J. Park, W. Kwon, and W. Hong, "Optically transparent 1-D EBG antenna using sub-skin depth thin-film alloy in the Ka-band," in *Proc. 13th Eur. Conf. Antennas Propag. (EuCAP)*, Mar. 2019, pp. 1–3.

[4] D. You, X. Wang, H. Herdian, X. Fu, H. Lee, M. Ide, C. D. Gomez, Z. Li, J. Mayeda, D. Awaji, J. Pang, H. Sakamoto, K. Okada, and A. Shirane, "A Ka-band deployable active phased array transmitter fabricated on 4-layer liquid crystal polymer substrate for small-satellite mount," *IEEE Access*, vol. 11, pp. 69522–69535, 2023.

[5] S. I. H. Shah, S. Bashir, M. Ashfaq, A. Altaf, and H. Rmili, "Lightweight and low-cost deployable origami antennas—A review," *IEEE Access*, vol. 9, pp. 86429–86448, 2021.

[6] H. A. E. Elobaid, S. K. Rahim, M. Himdi, X. Castel, and M. A. Kasgari, "A transparent and flexible polymer-fabric tissue UWB antenna for future wireless networks," *IEEE Antennas Wireless Propag. Lett.*, vol. 16, pp. 1333–1336, 2017.

[7] H. Suzuki and T. Kamijo, "Millimeter-wave measurement of complex permittivity by perturbation method using open resonator," *IEEE Trans. Instrum. Meas.*, vol. 57, no. 12, pp. 2868–2873, Dec. 2008.

[8] C. Easton, M. Jacob, and J. Krupka, "Non-destructive complex permittivity measurement of low permittivity thin film materials," *Meas. Sci. Technol.*, vol. 18, no. 9, p. 2869, 2007.

[9] Y. Kato and M. Horibe, "Broadband permittivity measurements up to 170-GHz using balanced-type circular-disk resonator excited by 0.8-mm coaxial line," *IEEE Trans. Instrum. Meas.*, vol. 68, no. 6, pp. 1796–1805, Jun. 2019.

[10] S. Rodini, S. Genovesi, G. Manara, and F. Costa, "Electromagnetic characterization of thin films by using non-contacting waveguides," *IEEE Trans. Antennas Propag.*, vol. 70, no. 9, pp. 8452–8460, Sep. 2022.

[11] L. Nov and J.-Y. Chung, "Dielectric property characterisation of thin films based on iterative comparisons of full-wave simulations and measurements," *IET Sci., Meas. Technol.*, vol. 14, no. 10, pp. 992–996, Dec. 2020.

[12] Y. Seo, C. Lee, I. Moon, K. Ota, R. Omote, and S. Kahng, "A planar millimeter-wave resonator-array to sense the permittivity of COP film with the 5G handset back-cover," *Sensors*, vol. 21, no. 13, p. 4316, Jun. 2021.

[13] P. G. Bartley and S. B. Begley, "Improved free-space S-parameter calibration," in *Proc. IEEE Instrumentationand Meas. Technol. Conf.*, vol. 1, May 2005, pp. 372–375.

[14] S. Trabelsi and S. O. Nelson, "Nondestructive sensing of physical properties of granular materials by microwave permittivity measurement," *IEEE Trans. Instrum. Meas.*, vol. 55, no. 3, pp. 953–963, Jun. 2006.

[15] F. Gonçalves, A. Pinto, R. Mesquita, E. Silva, and A. Brancaccio, "Free-space materials characterization by reflection and transmission measurements using frequency-by-frequency and multi-frequency algorithms," *Electronics*, vol. 7, no. 10, p. 260, Oct. 2018.

[16] G. L. Friedsam and E. M. Biebl, "A broadband free-space dielectric properties measurement system at millimeter wavelengths," *IEEE Trans. Instrum. Meas.*, vol. 46, no. 2, pp. 515–518, Apr. 1997.

[17] D. Bourreau, A. Peden, and S. Le Maguer, "A quasi-optical free-space measurement setup without time-domain gating for material characterization in the *W*-band," *IEEE Trans. Instrum. Meas.*, vol. 55, no. 6, pp. 2022–2028, Dec. 2006.

[18] D. K. Ghodgaonkar, V. V. Varadan, and V. K. Varadan, "A free-space method for measurement of dielectric constants and loss tangents at microwave frequencies," *IEEE Trans. Instrum. Meas.*, vol. 38, no. 3, pp. 789–793, Jun. 1989.

[19] D. K. Ghodgaonkar, N. A. Ali, and L. Giubbolini, "Microwave non-destructive testing of composite materials using free-space microwave measurement techniques," in *Proc. 15th World Conf. Non-Destructive Testing*, 2000, pp. 15–21.

[20] P. G. Bartley and S. B. Begley, "A new free-space calibration technique for materials measurement," in *Proc. IEEE Int. Instrum. Meas. Technol. Conf.*, May 2012, pp. 47–51.

[21] E. Hajisaeid, A. F. Dericioglu, and A. Akyurtlu, "All 3-D printed free-space setup for microwave dielectric characterization of materials," *IEEE Trans. Instrum. Meas.*, vol. 67, no. 8, pp. 1877–1886, Aug. 2018.

[22] S.-S. Cho, D. Yoon, J. Kim, N. Yoon, K. H. Oh, D. W. Woo, Y. B. Park, and I.-P. Hong, "Millimeter-wave band frequency-selective radome design with angle of incidence stability," *J. Korean Inst. Electromagn. Eng. Sci.*, vol. 33, no. 5, pp. 340–347, May 2022.

[23] D. Yoon, D.-Y. Na, and Y. B. Park, "Design and fabrication of tapered dielectric for broadband and wide incident angle transmission," *IEEE Trans. Antennas Propag.*, vol. 70, no. 12, pp. 11922–11933, Dec. 2022.

[24] M. S. Hilario, B. W. Hoff, B. Jawdat, M. T. Lanagan, Z. W. Cohick, F. W. Dynys, J. A. Mackey, and J. M. Gaone, "*W*-band complex permittivity measurements at high temperature using free-space methods," *IEEE Trans. Compon., Packag., Manuf. Technol.*, vol. 9, no. 6, pp. 1011–1019, Jun. 2019.

[25] A. Arsenovic, J. Hillairet, J. Anderson, H. Forstén, V. Rieß, M. Eller, N. Sauber, R. Weikle, W. Barnhart, and F. Forstmayr, "Scikit-RF: An open source Python package for microwave network creation, analysis, and calibration [speaker's corner]," *IEEE Microw. Mag.*, vol. 23, no. 1, pp. 98–105, Jan. 2022.

[26] A. M. Nicolson and G. F. Ross, "Measurement of the intrinsic properties of materials by time-domain techniques," *IEEE Trans. Instrum. Meas.*, vol. IM-19, no. 4, pp. 377–382, Nov. 1970.

[27] Z. Chen and Z. Xiong, "Mitigation of band edge effects in Fourier transform based time domain gating," in *Proc. 13th Eur. Conf. Antennas Propag. (EuCAP)*, Mar. 2019, pp. 1–5.

[28] G. Dhondt, D. De Zutter, and L. Martens, "An improved free-space technique modelling for measuring dielectric properties of materials," in *IEEE Antennas Propag. Soc. Int. Symp. Dig.*, vol. 1, Jul. 1996, pp. 180–183.

[29] *Uncertainty of Measurement—Part 3: Guide To the Expression of Uncertainty in Measurement (GUM:1995)*, Standard ISO/IEC Guide 98-3:2008, International Organization for Standardization, 2008.

[30] M. Born and E. Wolf, *Principles of Optics: Electromagnetic Theory of Propagation, Interference and Diffraction of Light*. Amsterdam, The Netherlands: Elsevier, 2013.

[31] M. J. D. Powell, "Restart procedures for the conjugate gradient method," *Math. Program.*, vol. 12, no. 1, pp. 241–254, Dec. 1977.

[32] W. H. Press, *Numerical Recipes: The Art of Scientific Computing*, 3rd ed., Cambridge, U.K.: Cambridge Univ. Press, 2007.

[33] P. Virtanen et al., "SciPy 1.0: Fundamental algorithms for scientific computing in python," *Nature Methods*, vol. 17, no. 3, pp. 261–272, 2020.

[34] J. Baker-Jarvis, R. G. Geyer, C. A. Grosvenor, C. L. Holloway, M. D. Janezic, R. T. Johnk, P. Kaboš, and J. Baker-Jarvis, "Measuring the permittivity and permeability of lossy materials: Solids, liquids, metals, building materials, and negative-index materials," Nat. Inst. Standards Technol., Boulder, CO, USA, Tech. Rep. 1536, 2005.

[35] Y. Hasegawa, Y. Ohki, K. Fukunaga, M. Mizuno, and K. Sasaki, "Complex permittivity spectra of various insulating polymers at ultrawide-band frequencies," *Electr. Eng. Jpn.*, vol. 198, no. 3, pp. 11–18, 2017.

[36] D. Yoon, J. H. Kim, N. Yoon, K. H. Oh, D. W. Woo, and Y. B. Park, "Time-gated free-space measurement signal processing method to estimate dielectric constant of 3D printed materials," *J. Korean Inst. Electromagn. Eng. Sci.*, vol. 33, no. 6, pp. 498–508, Jun. 2022.

DAEYEONG YOON (Member, IEEE) received the B.S. degree in electrical and computer engineering and the integrated M.S./Ph.D. degree in AI convergence network from Ajou University, Suwon-si, South Korea, in 2018 and 2024, respectively. Since 2024, he has been a Postdoctoral Researcher with Ajou University. His research interests include periodic structures, frequency-selective surfaces, radomes, and radar cross-sections.

JIHYUNG KIM (Member, IEEE) received the B.S. and integrated M.S./Ph.D. degrees in electrical and computer engineering from Ajou University, Suwon-si, South Korea, in 2009 and 2016, respectively. Since 2016, he has been a Researcher with Hanwha Systems, Yongin-si, South Korea. His research interests include the analysis of aperture array antennas and radomes.

DONG-YEOP NA (Member, IEEE) received the B.S. and M.S. degrees in electrical and computer engineering from Ajou University, Suwon-si, South Korea, in 2012 and 2014, respectively, and the Ph.D. degree in electrical and computer engineering from The Ohio State University, Columbus, OH, USA, in 2018. From 2019 to 2022, he was with the Elmore Family School of Electrical and Computer Engineering, Purdue University, West Lafayette, IN, USA, as a Postdoctoral Research Associate and a Research Scientist. He joined the Department of Electrical Engineering, Pohang University of Science and Technology, Pohang-si, South Korea, in 2022, where he is currently an Assistant Professor. His research interests include computational electromagnetics, kinetic plasma modeling via particle-in-cell algorithms, and quantum electromagnetics.

YONG BAE PARK (Senior Member, IEEE) received the B.S., M.S., and Ph.D. degrees in electrical engineering from Korea Advanced Institute of Science and Technology, South Korea, in 1998, 2000, and 2003, respectively. From 2003 to 2006, he was with Korea Telecom Laboratory, Seoul, South Korea. He joined the School of Electrical and Computer Engineering, Ajou University, South Korea, in 2006, where he is currently a Professor. His research interests include electromagnetic field analysis, high-frequency methods, metamaterial antennas, radomes, and stealth technology.